Selection Rules for Bloch Wave Scattering for HREM Imaging of Imperfect Crystals Along Symmetry Axes

Peter D Nellist, Eireann C Cosgriff, Peter B Hirsch, D J H Cockayne

Selection Rules for Bloch Wave Scattering for HREM Imaging of Imperfect Crystals Along Symmetry Axes

Journal:	*Philosophical Magazine & Philosophical Magazine Letters*
Manuscript ID:	TPHM-07-Aug-0246.R1
Journal Selection:	Philosophical Magazine
Date Submitted by the Author:	14-Oct-2007
Complete List of Authors:	Nellist, Peter; University of Oxford, Department of Materials Cosgriff, Eireann; University of Oxford, Department of Materials Hirsch, Peter; University of Oxford, Department of Materials Cockayne, D; University of Oxford, Department of Materials; University of Oxford, Department of Materials
Keywords:	electron diffraction, HREM, strain
Keywords (user supplied):	electron diffraction, HREM, strain

Selection Rules for Bloch Wave Scattering for HREM Imaging of Imperfect Crystals Along Symmetry Axes

P. D. NELLIST†*, E. C. COSGRIFF†, P. B. HIRSCH† and D. J. H. COCKAYNE†

†Department of Materials, University of Oxford, Parks Road, Oxford, OX1 3PH, UK

Correspondence *Corresponding author. Email: Peter.Nellist@materials.ox.ac.uk

A Bloch wave analysis is used to investigate high-resolution electron microscope (HREM) imaging of crystals containing atomic displacements due to strain. In the absence of interband scattering, the shifts of peaks and troughs in the image will correspond to the displacements of the atoms in the exit surface. Interband scattering will shift the image peaks away from the actual atom positions and modify the apparent magnitude of the displacement identified by the observed image peak positions. By considering the case of seven-beam imaging of a cubic crystal aligned along a <111> axis, it is shown that the symmetry of the Bloch waves lead to selection rules for the interband scattering, similar to those seen for dipole electron excitations in atoms. It is also shown that, to first order, no intraband scattering can occur.

Keywords: HREM; electron diffraction; strain

1 Introduction

High resolution electron microscopy (HREM) imaging of crystals is generally carried out along a symmetry axis, where the density of the atoms along columns parallel to the viewing direction and the spacing of the atomic columns tend to be large. For perfect crystals the columns parallel to the viewing directions are straight, but if the crystals contain defects this may no longer be the case. Examples include small clusters of impurity atoms acting as strain centres, small dislocation loops, dislocations inclined to the viewing direction, and surface relaxation strain around dislocations normal to the sample surface. Such atomic displacements, $\mathbf{R}(z)$ where z is the depth in the crystal, result in shifts of the peaks and troughs of intensity in the image relative to those for the perfect crystals, and also give rise to diffraction contrast, which can be used for example to locate end-on screw dislocations which would otherwise be difficult to see.

This paper addresses the question of how the atomic displacements **R** which are a function of z affect the peaks and troughs of intensity in the HREM image. It is of course possible to simulate the HREM images of imperfect crystals by the multislice method using standard codes [1], but such computer simulations do not elucidate the basic physical processes which result in the changes in the intensity distribution in the image due to the imperfection. For example, in recent work by Mendis et al. [2] on the use of the Nye tensor in analysing HREM images of screw dislocations in body-centred cubic (bcc) Mo, viewed end-on, the authors carried out simulations of HREM images of a screw dislocation along a [111] axis, normal to the surfaces of elastically isotropic thin foils, whose surface stresses were relaxed by applying the Eshelby twist displacements [3]. The Eshelby twist displacements are of opposite sign at the entrance and exit surfaces. The image simulations showed displacements of the image peaks from the actual atom positions in the perfect lattice a) whose signs were the same as and b) whose magnitudes were smaller than those expected from the Eshelby twist displacements at the exit surface. But the explanation of these results was not clear.

In this paper we present a Bloch wave analysis of the scattering processes with a view to elucidating the underlying physical mechanisms leading to peak displacements in HREM images. We consider a bcc crystal viewed along the <111> axis and containing a defect causing displacements which are a function of z. By considering a 7-beam case, consisting of the direct beam plus the six surrounding 110-type reflections, we shall show that certain general selection rules apply for the Bloch wave scattering. In a subsequent paper these results are applied to explain the nature of the image simulations of the Eshelby twist displacements associated with a screw dislocation in a bcc crystal viewed end-on in a thin foil. The selection rules derived here also apply to other cases in which the diffraction pattern can be treated as a direct beam surrounded by a number of symmetry-related diffraction spots, for example the 5-beam case for cubic crystals (primitive, body-centred or face-centred) viewed along the <100> or the 7-beam case for cubic <111> axes. In

subsequent work we will examine the extent to which this approach can be extended to more complicated crystal structures, such as those with a basis of more than one atom.

Throughout this paper we assume that the peaks observed in the HREM image correspond to the peaks in the electron intensity at the exit-surface of the sample. Recent investigations have made use of exit-surface wave reconstruction (for example [4]), for which the present analysis is particularly relevant. Here we consider how the image feature shifts may not exactly correspond to the displaced atom positions because of interband scattering.

2 Bloch wave scattering

We follow the usual Bloch wave approach to high-energy electron diffraction as described in detail many times previously (see for example [5]). This approach allows the wave function $\omega(\mathbf{r}, z)$ in the perfect periodic crystal to be written in terms of a series of plane Bloch waves of excitation ψ^i

$$\omega(\mathbf{r}, z) = \sum_i \psi^i b^i(\mathbf{r}) \exp\left(2\pi i k_z^i z\right) \qquad (1a),$$

where

$$b^i(\mathbf{r}) = \sum_{\mathbf{g}} C_{\mathbf{g}}^i \exp\left(2\pi i\left(\mathbf{k}_t + \mathbf{g}\right)\cdot \mathbf{r}\right) \qquad (1b),$$

where $\mathbf{k}_t$ is the transverse component of the incident wave vector. The longitudinal component of the wave vectors $k_z^i = K_z + \gamma^i$, where K_z is the z component of the incident beam wave vector after correction for the mean inner potential and γ^i is the change in wave vector associated with the i^{th} branch of the dispersion surface [5]. The values of the Fourier coefficients, $C_{\mathbf{g}}^i$, are determined by the deviation parameters for the different branches, and the Bloch wave excitations, ψ^i, by the boundary conditions. For a non-absorbing crystal the $C_{\mathbf{g}}^i$'s are real, and the excitation of the wave $\psi^i = C_0{}^i$.

For the diffraction conditions described here, the symmetry imposes certain conditions on the nature and excitation of the Bloch waves. Thus, it is easy to show by methods described in [5], that if the origin is taken at a centre of symmetry, for the case considered in [2], where 6 equivalent 110 reflections are assumed to contribute to the image, there will be 7 Bloch waves, two of which, waves 1 and 2, with excitations ψ^1 and ψ^2, have Fourier coefficients $C_{\mathbf{g}}^1$ and $C_{\mathbf{g}}^2$ which are independent of **g** for all **g** except **g**=000, i.e. they correspond to symmetrical waves with their peaks or troughs centred at the origin (which for simple structures such as Mo coincides with the position of columns of atoms). These are the only two Bloch waves which are excited. The others, waves 3 - 7, have Fourier coefficients of both signs, and have peaks or troughs between the atomic columns. Because of symmetry conditions they are not excited, which can be seen by noting that their **g**=000 component is zero. The $C_{\mathbf{g}}^i$ matrix is shown in Table 1. Mendis (private communication) has derived a similar matrix including the effects of absorption. In our derivation, we have neglected absorption to make the symmetry immediately apparent. The analysis shows waves 3 and 4, and 5 and 6 to be degenerate, i.e. 3 and 4 belong to one branch of the dispersion surface, and 5 and 6 to another. The initial use of the symmetry operation produces complex values of $C_{\mathbf{g}}^i$ for these waves, but by adding and subtracting these $C_{\mathbf{g}}^i$'s for a degenerate pair, two alternative orthogonal sets of real $C_{\mathbf{g}}^i$'s are generated which satisfy the equations of the dynamical theory [5]. These values are shown in the table.

We note that waves 3 and 4 are antisymmetric, with the $C_{\mathbf{g}}^i$ coefficients satisfying a $\bar{1}$ inversion axis relation. Waves 5 and 6 are symmetric, consistent with diad symmetry along the zone axis. Wave 7 has $\bar{3}$ symmetry; it consists of three sine (i.e. antisymmetric) waves with wave vectors at 120^0 relative to each other. However, for waves 3, 4, 5, 6 and 7, the amplitude at the centre of the atom columns is zero.

The symmetry of these Bloch wave states can also be described by analogy with the symmetry of atomic orbitals. Thus waves 1 and 2 have s-like symmetry, and we allocate to them a quantum number (for angular momentum) $l = 0$. Waves 3 and 4 have p-like symmetry with $l = 1$. Waves 5 and 6 have d-like symmetry with $l = 2$. Wave 7 has f-like symmetry with $l = 3$.

Figure 1 shows the spatial distribution of the amplitude and intensity (inset) of the Bloch waves for illumination along the symmetry axis [111], and superimposed on atom columns of a bcc lattice passing through the lattice points. Positive and negative amplitudes are indicated by + and - on the figures. The distribution of amplitudes for waves 3 to 7 can be obtained directly from the $C_{\mathbf{g}}^{i}$'s in the table. To obtain the solutions for waves 1 and 2 the equations of the dynamical theory have to be solved (see Chapter 12 of [5]). For bcc Mo, viewed along [111], with a 300kV electron beam the results are $A^1 = 0.5369$, $B^1 = 0.3444$, $A^2 = 0.8437$ and $B^2 = -0.2192$. It is clear from the figures that only wave 1 channels down the atomic columns, the others channel between the atoms, as pointed out by Mendis (private communication). These figures show clearly the symmetry of the Bloch waves, in particular the s-type symmetry of Bloch waves 1 and 2 and the p-type symmetry of Bloch waves 3 and 4. The form of these waves can be easily obtained from the $C_{\mathbf{g}}^{i}$'s in the table. Bloch waves 1 and 2 are symmetrical, and are given by

$$b^i(\mathbf{r}) = A^i + 2B^i\left(\cos\left(2\pi\mathbf{g}_{110}\cdot\mathbf{r}\right)+\cos\left(2\pi\mathbf{g}_{011}\cdot\mathbf{r}\right)+\cos\left(2\pi\mathbf{g}_{\bar{1}01}\cdot\mathbf{r}\right)\right) \quad (2),$$

where $i = 1$ or 2 respectively. Waves 3 and 4 are in the form of two modulated sine waves along <110> and <211> directions at 90 degrees to each other.

Thus

$$b^3(\mathbf{r}) = \sum_{\mathbf{g}} C_{\mathbf{g}}^3 \exp(2\pi i \mathbf{g}.\mathbf{r}) = (2i/\sqrt{3})\sin(\pi \mathbf{g}_{110}.\mathbf{r})[2\cos(\pi \mathbf{g}_{110}.\mathbf{r}) + \cos(\pi \mathbf{g}_{\bar{1}12}.\mathbf{r})] \quad (3),$$

and

$$b^4(\mathbf{r}) = \sum_{\mathbf{g}} C_{\mathbf{g}}^4 \exp(2\pi i \mathbf{g}.\mathbf{r}) = 2i \sin(\pi \mathbf{g}_{\bar{1}12} \cdot \mathbf{r})\cos(\pi \mathbf{g}_{110} \cdot \mathbf{r}) \quad (4),$$

using the indexing of the reflections in the table. In plotting Fig. 1, we have ignored the *i* prefactor in (3) and (4), which is an arbitrary phase factor.

Now consider an imperfect crystal in which there are variable displacements **R**(z) along any column. Then cutting the crystal into thin slices normal to the viewing direction, and applying the column approximation [5], each slice is considered as a perfect crystal with the lattice displaced by a displacement **R**(z) for the particular column being considered. In general the wave function incident on a given slice will find that the atoms have been displaced relative to the previous slice by a distance that we assume is small compared to a lattice spacing. The Bloch waves in the displaced slice are also displaced with the lattice, and are excited by a wave leaving the previous slice that is no longer symmetric with respect to the atom sites. This can lead to interband and intraband scattering. Near the entrance surface the incident wave, consisting of Bloch waves 1 and 2, is symmetrical. Because **R**(z) destroys the symmetry, the resulting wave must have Fourier components which are antisymmetrical, and which satisfy $\bar{1}$ type symmetry. Since the resulting wave is a composition of the Bloch waves, Bloch waves 1 and 2, the only waves excited at the entrance surface, cannot contribute to this asymmetry. Consequently there is no intraband scattering, neither is there interband scattering between these two waves. Furthermore, the only Bloch waves with $\bar{1}$ symmetry are waves 3 and 4. It follows that near the entrance surface the only scattering possible is from the symmetrical waves 1 and 2 to the antisymmetrical waves 3 and 4 with $\bar{1}$ symmetry. This conclusion is proved in section 3. We note that

these are vertical transitions in the dispersion diagram, and that there is no lateral movement along a dispersion surface.

The HREM image will be determined by the wave function propagating in the last slice of crystal at the exit surface. In the absence of interband scattering, the observed peaks occur at the atom positions in the final slice, and these may be displaced relative to those of the perfect crystal depending on the nature of the defect. Because of the cumulative interband scattering from the symmetrical waves 1 and 2 to the antisymmetrical waves 3 and 4 (we neglect any scattering from waves 3 and 4 to waves 5 and 6 and from 5 and 6 to 7), the peaks and troughs in the total wave function will shift from the atomic positions by an amount depending on the strength of the interband scattering. If this is not too large, the apparent displacements observed in the HREM image will be mainly determined by waves 1 and 2 and so have the same direction as those of the actual displacements at the exit surface. However the magnitude of the apparent displacements will be different from the actual displacements, reflecting the effect of the cumulative interband scattering in the rest of the crystal between the two surfaces due to displacements relative to the atomic positions at the exit surface. In a following paper these considerations will be applied to the case where $\mathbf{R}(z)$ is due to the Eshelby twist.

3. Expressions for intraband and interband scattering

Equation 12.25 in [5] gives the n-beam Howie-Whelan equation in terms of Bloch wave excitations ψ^i. If $\mathbf{\Psi}$ is a column matrix of the wave excitations,

$$\frac{d}{dz}\mathbf{\Psi} = 2\pi i\left\{\exp\left(-2\pi i\gamma^i z\right)\right\}\mathbf{C}^{-1}\left\{\beta'_g\right\}\mathbf{C}\left\{\exp\left(2\pi i\gamma^i z\right)\right\}\mathbf{\Psi} \qquad (5)$$

The $\mathbf{C}$ and $\mathbf{C}^{-1}$ matrices are evaluated for the perfect crystal, and $\beta'_{\mathbf{g}} = \frac{d}{dz}\left(\mathbf{g}.\mathbf{R}(z)\right)$. Curly brackets define diagonal matrices. Neglecting absorption $\mathbf{C}$ and $\mathbf{C}^{-1}$ are real. For a crystal, the smallest interval, dz, in

equation (5) is an interatomic distance, and for (5) to hold the change in displacement must be small over this distance; a condition likely to be valid for small elastic strain fields. On evaluating the matrices we find

Intraband scattering $$\left(\frac{d\psi^i}{dz}\right)_{i->i} = 2\pi i \sum_{\mathbf{g}\neq 0} \left(C_{\mathbf{g}}^i\right)^2 \beta'_{\mathbf{g}} \psi^i \qquad (6).$$

Interband scattering $$\left(\frac{d\psi^j}{dz}\right)_{i->j} = 2\pi i \sum_{\mathbf{g}\neq 0} \beta'_{\mathbf{g}} C_{\mathbf{g}}^j C_{\mathbf{g}}^i \exp\left(2\pi i \Delta k^{ij} z\right)\psi^i \qquad (7),$$

where $\Delta k^{ij} = k^i - k^j$.

Consider now the intraband scattering in equation (6) for the [111] zone axis case in Mo, with six 110 type reflections operating. As stated in section 2, because of symmetry conditions, only Bloch waves 1 and 2 are excited. Thus the intraband scattering for wave 1 is given by

$$\left(\frac{d\psi^1}{dz}\right)_{1->1} = 2\pi i \sum_{\mathbf{g}\neq 0} \left(C_{\mathbf{g}}^{\ 1}\right)^2 \frac{d}{dz}\left(\mathbf{g}.\mathbf{R}(z)\right)\psi^1 \qquad (8).$$

But again because of the symmetry all the $C_{\mathbf{g}}^{\ 1}$ values are equal. Hence

$$\left(\frac{d\psi^1}{dz}\right)_{1->1} = 2\pi i \left(C_{\mathbf{g}}^{\ 1}\right)^2 \sum_{\mathbf{g}} \left(\mathbf{g}.\frac{d\mathbf{R}(z)}{dz}\right)\psi^1 = 2\pi i \left(C_{\mathbf{g}}^{\ 1}\right)^2 \frac{d\mathbf{R}(z)}{dz}\cdot \sum_{\mathbf{g}} \mathbf{g}\psi^1 = 0 \qquad (9),$$

since **+g** and **-g** cancel out for the 3 pairs of reflexions. Similarly $\left(\frac{d\psi^2}{dz}\right)_{2->2} = 0$. More generally, we note that for all Bloch waves $\left(C_{\mathbf{g}}^i\right)^2 = \left(C_{-\mathbf{g}}^i\right)^2$ for **g**≠000, and hence the contribution from **+g** and **–g** cancel out. Thus there is no intraband scattering for any of the waves.

For the interband scattering from 1 to 2 we get from equation (7)

$$\left(\frac{d\psi^2}{dz}\right)_{1->2} = 2\pi i \sum_{\mathbf{g}} \beta'_{\mathbf{g}} C_{\mathbf{g}}{}^2 C_{\mathbf{g}}{}^1 \exp\left(2\pi i \Delta k^{12} z\right)\psi^1 \qquad (10)$$

But again because all $C_{\mathbf{g}}{}^1$ and $C_{\mathbf{g}}{}^2$ values are equal for waves 1 and 2 respectively, the above sum over **g** is simply a sum over $\beta'_{\mathbf{g}}$ which is zero.

Hence $$\left(\frac{d\psi^2}{dz}\right)_{1->2} = \left(\frac{d\psi^1}{dz}\right)_{2->1} = 0 \qquad (11)$$

We also find that $$\left(\frac{d\psi^5}{dz}\right)_{1,2->5} = \left(\frac{d\psi^6}{dz}\right)_{1,2->6} = \left(\frac{d\psi^7}{dz}\right)_{1,2->7} = \left(\frac{d\psi^7}{dz}\right)_{3,4->7} = 0 \qquad (12).$$

On the other hand, we find that transitions from waves 1 and 2 to 3 and 4 are possible. Thus, near the entrance surface, because of the symmetry, the only scattering possible is from waves 1 and 2 to 3 and 4. With increasing depth, when ψ^3 and ψ^4 become finite, further scattering can occur from 3 and 4 to 5 and 6, and then from 5 and 6 to 7. The permitted interband scattering transitions are consistent with the selection rule for the orbital quantum numbers of $\Delta l = \pm 1$. The derivation of this selection rule is similar to that seen for dipole transitions between atomic orbitals. From [5] we note that waves with a symmetry identified by l are formed by the linear combinations of waves that have Fourier components

$$C_{\mathbf{g}} = \exp\left(\pm i l \phi_{\mathbf{g}}\right) \qquad (13)$$

for all components except **g**=000. The angle $\phi_{\mathbf{g}}$ is the azimuthal angle between the vector **g** and an arbitrary reference axis (the $\phi_{\mathbf{g}}$=0 axis) that we take as being along one reciprocal lattice vector. For the 7-beam case considered here the $\phi_{\mathbf{g}}$ angles take the values $m\pi/3$, where m is an integer. Consider now the transition from a state with symmetry l_1 to one with symmetry l_2. If the angle between $\frac{d\mathbf{R}}{dz}$ and the $\phi_{\mathbf{g}}$=0 axis is η, $\mathbf{g}\cdot\frac{d\mathbf{R}}{dz} = |\mathbf{g}|\left|\frac{d\mathbf{R}}{dz}\right|\cos(\phi_{\mathbf{g}}-\eta)$ and equation (7) can then be written as a sum over the 6 diffracted beams, with m=0 corresponding to the reference **g**,

$$\left(\frac{d\psi^{l_2}}{dz}\right) = 2\pi i|\mathbf{g}|\left|\frac{d\mathbf{R}}{dz}\right|\exp\left(2\pi i\Delta k^{l_1l_2}z\right)\psi^{l_1}\sum_{m=0}^{5}\exp\left(il_1m\pi/3\right)\exp\left(-il_2m\pi/3\right)\cos\left(m\pi/3-\eta\right) \quad (14).$$

Expanding the cosine gives two terms

$$\begin{aligned}\left(\frac{d\psi^{l_2}}{dz}\right) &= 2\pi i|\mathbf{g}|\left|\frac{d\mathbf{R}}{dz}\right|\exp\left(2\pi i\Delta k^{l_1l_2}z\right)\psi^{l_1}\sum_{m=0}^{5}\exp\left(i(l_1-l_2)m\pi/3\right)\frac{1}{2}\left[\exp(m\pi/3-\eta)+\exp(-m\pi/3+\eta)\right]\\ &= 2\pi i|\mathbf{g}|\left|\frac{d\mathbf{R}}{dz}\right|\exp\left(2\pi i\Delta k^{l_1l_2}z\right)\psi^{l_1}\frac{1}{2}\sum_{m=0}^{5}\left[\exp\left(i(l_1-l_2+1)m\pi/3-\eta\right)+\exp\left(i(l_1-l_2-1)m\pi/3+\eta\right)\right]\end{aligned} \quad (15),$$

but $\sum_{m=0}^{5}\exp\left(ilm\pi/3+\eta\right)=0$ for all integer l except l=0, and therefore for (14) to have a finite value $\Delta l = l_1-l_2 = \pm 1$. Note that a similar approach can be taken for other symmetries, for example the 5-beam case.

There can be further selection rules which depend on $\beta'_{\mathbf{g}}$. For example, for interband scattering from wave 1 to wave 3, from equation (7) and the $C^i_{\mathbf{g}}$'s we find

$$\left(\frac{d\psi^3}{dz}\right)_{1->3} = 2\pi i\sqrt{3}B^1\beta'_{110}\exp\left(2\pi i\Delta k^{13}z\right)\psi^1 \quad (16),$$

so that if $\beta'_{110} = 0$, resulting from a displacement perpendicular to **g**=110, $\psi^3 = 0$. The same conclusion follows for scattering from 2 to 3. It follows that in this case interband scattering is possible only from 1 or 2 to 4. If $\psi^3 = 0$, and the scattering to ψ^4 is small, the total wave function, including the phase factors, at the exit face $z = t$ is

$$\omega(\mathbf{r},t) = \psi^1 b^1(\mathbf{r}) \exp\left(2\pi i k_z^1 t\right) + \psi^2 b^2(\mathbf{r}) \exp\left(2\pi i k_z^2 t\right) + \left(\psi^4_{1->4} + \psi^4_{2->4}\right) b^4(\mathbf{r}) \exp\left(2\pi i k_z^4 t\right) \quad (17)\,,$$

where ψ^1 and ψ^2 are approximately the excitations in the perfect crystal. It is easy to see from the nature of wave 4 (see equation (4)), that the peak intensities in the image will be shifted along $\left[\bar{1}\,12\right]$, in a direction depending on the sign of the sine wave. But the magnitude and direction i.e. whether + or - $\left[\bar{1}\,12\right]$, of the observed image shift relative to the atom positions at the exit face will depend on the phase factors and thickness. We shall examine this in detail for the Eshelby twist elsewhere.

4 Conclusions

For HREM imaging along symmetry axes of crystals containing strain fields causing depth dependent lattice displacements, the image reflects the actual atomic displacements at the exit surface, but the image peaks may be shifted with respect to the atom positions due to interband scattering. We find that certain selection rules operate for interband scattering of Bloch waves. These rules have been established for images formed with a direct beam plus six 110 type reflections along [111] directions with triad symmetry in a bcc crystal. In the perfect crystal the excited Bloch waves are symmetrical, and the image intensity peaks coincide with the atoms at the lattice points. In an imperfect crystal interband scattering is initially allowed only to antisymmetrical p-type waves. If the interband scattering is small, the intensity peaks at the exit face are shifted from the atom positions at the exit face by the presence of the antisymmetrical waves by an amount depending on the strength of the scattering and the phase factors. This means that the apparent atom

displacements, identified by image peaks, may not correspond to the actual atom displacements at the exit face.

Acknowledgments

The authors would like to acknowledge useful discussions with Prof K J Hemker and Dr B Mendis. PBH thanks the Head of the Department of Materials, University of Oxford, for provision of facilities. PDN and EC thank the Department of Materials, University of Oxford, for funding.

References

[1] See, for example, E.J. Kirkland, *Advanced Computing in Electron Microscopy* (Plenum, New York, 1998)

[2] B.G. Mendis, Y. Mishin, C.S. Hartley and K.J. Hemker, Phil. Mag. **86** 4607. (2006); V. Vitek and B.G. Mendis (private communication).

[3] J.D. Eshelby and A.N. Stroh, Phil. Mag. **42** 1401 (1951).

[4] X. Xu, S. P. Beckman, P. Specht, et al., Phys. Rev. Lett. **95** 145501 (2005).

[5] P.B. Hirsch, A. Howie, R.B. Nicholson, D.W. Pashley and M.J. Whelan, *Electron Microscopy of Thin Crystals* (Butterworths, London, 1967).

Table 1. The $C_{\mathbf{g}}^{i}$ matrix for the symmetric 7-beam case.

	wave / **g**	1	2	3	4	5	6	7
	000	A^1	A^2	0	0	0	0	0
	110	B^1	B^2	$1/\sqrt{3}$	0	$1/\sqrt{3}$	0	$1/\sqrt{6}$
C =	011	B^1	B^2	$1/\sqrt{12}$	$1/2$	$-1/\sqrt{12}$	$1/2$	$-1/\sqrt{6}$
	$\bar{1}01$	B^1	B^2	$-1/\sqrt{12}$	$1/2$	$-1/\sqrt{12}$	-1/2	$1/\sqrt{6}$

	$\bar{1}\,\bar{1}\,0$	B^1	B^2	$-1/\sqrt{3}$	0	$1/\sqrt{3}$	0	$-1/\sqrt{6}$
	$0\,\bar{1}\,\bar{1}$	B^1	B^2	$-1/\sqrt{12}$	-1/2	$-1/\sqrt{12}$	1/2	$1/\sqrt{6}$
	$10\,\bar{1}$	B^1	B^2	$1/\sqrt{12}$	-1/2	$-1/\sqrt{12}$	-1/2	$-1/\sqrt{6}$

Figure 1. The spatial distribution of the amplitude and intensity (inset) of the Bloch waves for illumination along the symmetry axis [111], and superimposed on atom columns of a bcc lattice passing through the lattice points. Positive and negative amplitudes are indicated by + and - on the figures. The amplitude greyscales are scaled symmetrically either side of zero so that black and white correspond to equal magnitudes of opposite sign, with grey showing zero amplitude.

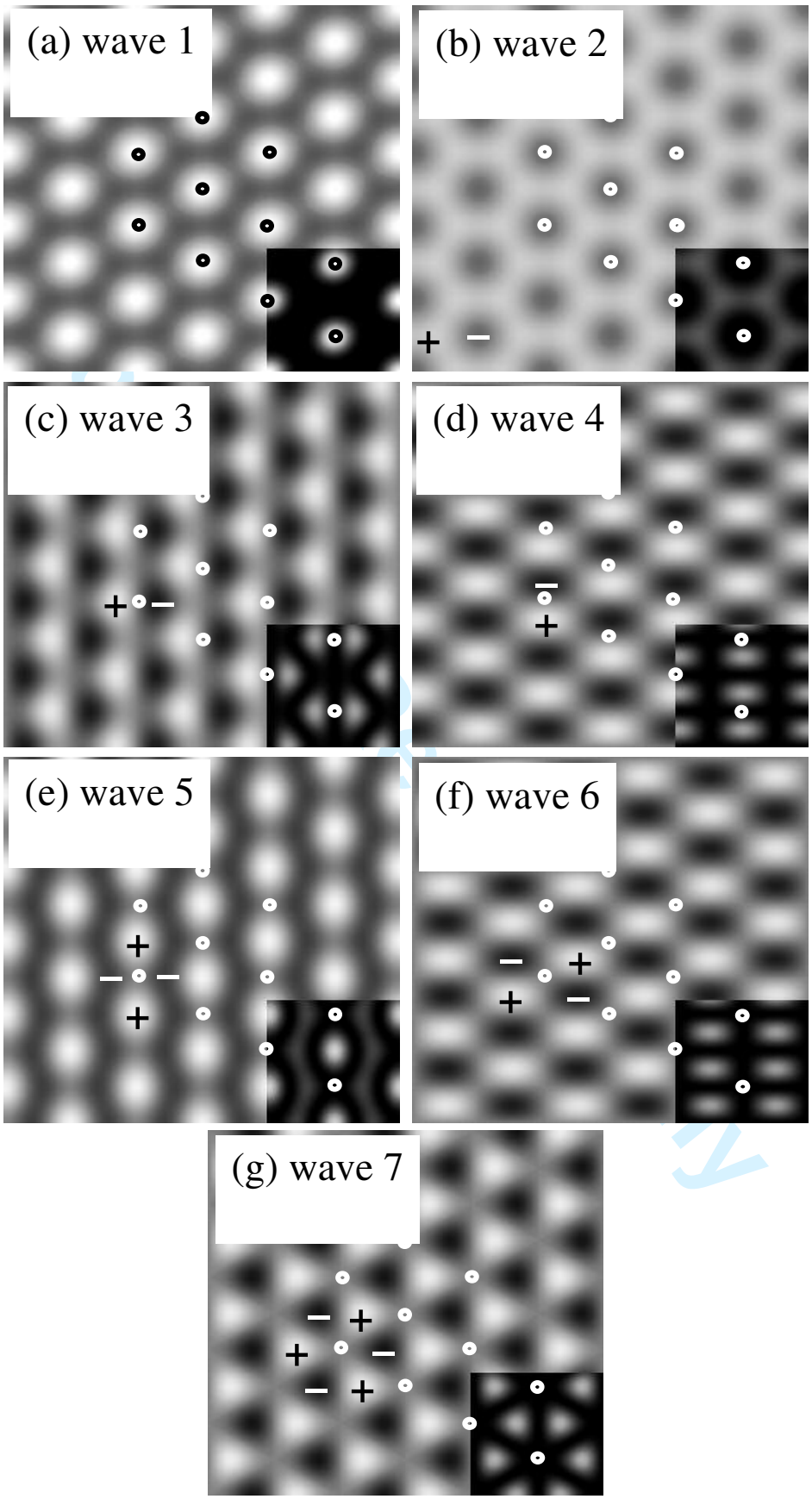
(a) wave 1
(b) wave 2
(c) wave 3
(d) wave 4
(e) wave 5
(f) wave 6
(g) wave 7